JOURNAL OF GUIDANCE, CONTROL, AND DYNAMICS
Vol. 16, No. 3, May-June 1993

Synthesis and Evaluation of an H_2 Control Law for a Hovering Helicopter

Marc D. Takahashi*
NASA Ames Research Center, Moffett Field, California 94035

The design and simulator evaluation of a rate-command flight-control law for a UH-60 helicopter in near-hover flight conditions are described. The multivariable control law was synthesized using an H_2 method, which, through weighting functions, directly shapes the singular values of the sensitivity $(I + GK)^{-1}$, complementary sensitivity $GK(I + GK)^{-1}$, and control input $K(I + GK)^{-1}$ transfer-function matrices. The design was implemented on the vertical motion simulator, and four low-speed hover tasks were used to evaluate the control system characteristics. The pilot comments indicated good decoupling and quick response characteristics, but also revealed a mild pilot-induced oscillation tendency in the roll axis.

Introduction

THE purpose of the research documented in this paper is to investigate the application of an H_2 multivariable design method to synthesize flight-control laws for helicopters. The objective of the work is to determine through analysis and piloted simulation the strengths and weaknesses of the H_2 method within the context of a modern rotorcraft design specification.

The choice of a multivariable design method is natural to the problem presented because of the highly coupled nature of helicopter dynamics and the desired level of feedback dictated by modern design specifications. Helicopter flight-control laws designed through classical single-input, single-output techniques are satisfactory when requirements do not infringe on the frequency range of significant interaxis cross coupling due to the rotor. Previous generation helicopters and their design requirements have complied with this assumption. However, future helicopters will use hingeless and bearingless rotors with more complex coupling, and these helicopters will have control-law design requirements demanding higher levels of feedback.

To ensure that the design criteria are sufficiently stringent to represent future requirements, the control law here was designed according to the Section 3 hover requirements in the Aeronautical Design Standard (ADS-33C).[1] Previous work on multivariable techniques for rotorcraft flight-control design[2-4] complied with part or none of the ADS-33C requirements, making these works difficult to interpret in terms of this new standard.

These previous works also used a low-order model (usually a 6-degree-of-freedom model) to design the flight-control law, and the final design was usually checked on a higher-order model in analysis or simulation. These higher-order models did not fully represent the rotor-fuselage dynamics, lacking either the coupled nature of the rotor dynamics (between the fuselage and the rotor and/or between the rotor degrees of freedom) or lacking the rotor lead-lag degree of freedom. These effects are known limiting factors in the feedback gains of helicopter flight-control laws and are represented in the analysis and piloted simulator model here. The importance of these effects was illustrated in advanced digital optical control system (ADOCS) research, where feedback gain reductions of 40% were necessary to avoid lead-lag instabilities.[5]

Received Nov. 22, 1991; revision received July 6, 1992; accepted for publication July 13, 1992. This paper is declared a work of the U.S. Government and is not subject to copyright protection in the United States.

*Aerospace Engineer, Aeroflightdynamics Directorate, U.S. Army Aviation Systems Command, MS-211-2. Member AIAA.

This paper continues with a description of the models used in the design process and piloted simulation, followed by a description of the method used to synthesize the flight-control law. The salient features of a rate-command control-law design are then discussed, followed by descriptions of the simulation environment and task arrangement. Finally, the results of the simulation are discussed and conclusions drawn. More details on the design method, design models, and flight-control design can be found in Ref. 6, whereas more details related to the simulation experiment can be located in Ref. 7.

Helicopter Models

The UH-60 is a utility helicopter with a four-bladed, articulated main rotor and is modeled for analysis and simulation using two distinct models: a linearized model and a nonlinear model.

The linearized model was used in the design method to derive the compensation and check closed-loop stability away from the design flight condition. The design flight condition is in hover at a gross weight of 16,800 lb, with the air density at a standard sea-level value of 0.00238 slug/ft^3 and the rotor speed fixed at 27 rad/s. There are 23 states in the design model, of which 8 states are attributable to the body motion, 12 states define the flap and lag motions of the rotor in nonrotating coordinates, and 3 states are used in the dynamic inflow model. Since the design condition is hover, the differential modes of the rotor are decoupled from the rigid-body dynamics and were removed from the model. The eigenvalues at the design flight condition are listed in Table 1. The matrices defining the linear model can be found in Ref. 6. The linearized model represents the helicopter as a 6-degree-of-

Table 1 Open-loop eigenvalues of helicopter model at the design flight condition

Eigenvalues	Description
$-0.2302 \pm j0.0175$	Heave + yaw
$0.2299 \pm j0.4280$	Longitudinal
$-0.1364 \pm j0.5270$	Lateral
-1.3479	Pitch
-4.8290	Roll
$-3.2684 \pm j4.2628$	Regressing flap
$-4.9144 \pm j5.3750$	Collective lag
$-5.7128 \pm j5.4340$	Differential lag
-19.3483	Inflow
$-4.2226 \pm j19.6360$	Regressing lag
$-24.5065 \pm j2.9036$	Inflow
$-8.6241 \pm j24.4865$	Collective flap
$-10.3668 \pm j25.2717$	Differential flap
$-5.7414 \pm j37.1472$	Progressing lag
$-9.3899 \pm j51.2472$	Progressing flap

freedom rigid fuselage, in straight and level flight, with rotor and lag degree of freedom.[8] The rotor-blade aerodynamic effects are modeled using two-dimensional, quasisteady strip theory, and a three-state Pitt/Peters dynamic inflow model. The blade lag-damper and fuselage aerodynamics of the model were matched to the characteristics of the UH-60. No rpm degree of freedom is included.

The nonlinear model[9] was used both to generate closed-loop time histories and as the model driving the ground-based simulator. This model also has blade flap and lag dynamics and includes a three-state Pitt/Peters inflow model. The linearized model differs from the nonlinear model in that the latter has the rotor rpm degree of freedom included along with a model of the T700 engine with an rpm governor. The nonlinear model is also a real-time model and uses approximations to speed up the processing of the system equations of motion. Forces and moments of various components (e.g., the rotor and fuselage) are calculated sequentially and, furthermore, the rotor and fuselage use different integration schemes to take advantage of the known properties of these components.

Control-Law Design Technique

The structure of the control-law design is shown in Fig. 1. The feedback properties of the design were obtained through the compensator $K(s)$, whereas the final response characteristics were obtained through the prefilter $P(s)$.

The compensator was chosen to minimize the performance index

$$J = E\left\{\lim_{T\to\infty}\frac{1}{T}\int_0^T y_1^T(t)y_1(t)\,dt\right\} = \frac{1}{2\pi}\int_{-\infty}^{+\infty} \times \mathrm{TR}[G_{11}(j\omega)G_{11}^H(j\omega)]\,d\omega = \|G_{11}\|_2^2 \tag{1}$$

where the integral on the right-hand side is the square of the H_2 norm of G_{11}. The function G_{11} is the u_1-to-y_1 transfer-function matrix of the system

$$\begin{pmatrix} y_1 \\ y_2 \end{pmatrix} = \left[\begin{array}{c|c} W_S(s) & -W_S(s)G(s) \\ 0 & W_W(s) \\ 0 & W_T(s)G(s) \\ \hline I & -G(s) \end{array}\right] \begin{pmatrix} u_1 \\ u_2 \end{pmatrix} \tag{2}$$

with the compensator connected via $u_2 = K(s)y_2$. Carrying out this operation results in the following equation.

$$y_1 = \begin{bmatrix} W_S(s)S_O(s) \\ W_W(s)W(s) \\ W_T(s)T_O(s) \end{bmatrix} u_1 = [G_{11}]u_1 \tag{3}$$

The transfer-function matrices W_S, W_W, and W_T are the frequency-dependent weight matrices and are used to control the shape of the sensitivity matrix $S_O = (I + GK)^{-1}$, the control input matrix $W = K(I + GK)^{-1}$, and the complementary sensitivity matrix $T_O = GK(I + GK)^{-1}$, respectively. Using Fig. 1, one will find that S_O is the transfer-function matrix from the disturbance to the tracking error $e = r - y$, whereas W is the transfer-function matrix from both the disturbance and noise to the control u. Therefore, reducing the effect of noise and disturbance on the tracking error and control activity requires reducing the size of S_O and W. The matrix T_O is

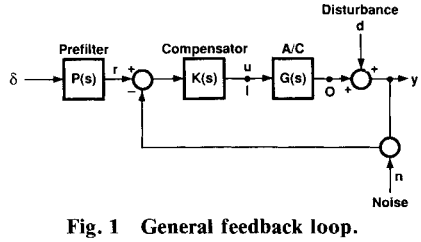

Fig. 1 General feedback loop.

the transfer function from the noise to the tracking error and is also related to the stability robustness of the closed-loop system. The latter relationship can be seen for an unstructured uncertainty model at the plant output Δ_O, which can be represented in Fig. 1 by inserting the transfer-function matrix $[I + \Delta_O]$ at point O. The well-known inequality

$$\bar{\sigma}[\Delta_O(j\omega)] \le 1/\bar{\sigma}[T_O(j\omega)] \tag{4}$$

guarantees stability and shows that reducing the destabilizing effect of large uncertainty requires reducing T_O in the appropriate frequency range.[10]

The calculation of $K(s)$ was done using matrix operations by converting Eq. (2) into the state-space form

$$\begin{pmatrix} \dot{x} \\ y_1 \\ y_2 \end{pmatrix} = \begin{bmatrix} A & B_1 & B_2 \\ C_1 & D_{11} & D_{12} \\ C_2 & D_{21} & D_{22} \end{bmatrix} \begin{pmatrix} x \\ u_1 \\ u_2 \end{pmatrix} \tag{5}$$

where the solution to minimize Eq. (1) can be found by solving two Riccati equations.[11] Full-state feedback gains K_c and Kalman filter gains K_f define the feedback compensation that is given by

$$K(s) = K_c(sI - A + B_2K_c + K_fC_2 - K_fD_{22}K_c)^{-1}K_f \tag{6}$$

The augmentation of the system with the various weight transfer-function matrices and the relatively large model both produce compensation of a large order. Reduction of the compensation was done using frequency-weighted balance realizations.[12]

The stability robustness of the compensation was considered throughout the design process. During the initial stages of the design, the approximate structure singular value μ_{app} was used as an indicator of any serious stability robustness problems. The approximate structured singular value is defined by

$$\mu_{\text{app}}[M] = \inf_D \|DMD^{-1}\|_F \tag{7}$$

which minimizes the Frobenius norm of DMD^{-1} over the diagonal and real-valued D matrix. This approximation is an upper bound on the structured singular value μ, and it is calculated using Osborne's method.[10] Two diagonal multiplicative uncertainty models were assumed: one at the plant input Δ_I and one at the plant output Δ_O. These models are represented in Fig. 1 by inserting either $[I + \Delta_I]$ at point I or $[I + \Delta_O]$ at point O. The value of $1/\mu[M(j\omega)]$ is the size of the smallest element of the uncertainty model that moves the closed-loop system to $j\omega$, which is marginal stability. For the input uncertainty model, the matrix M is $KG(I + KG)^{-1}$, whereas for the output uncertainty model, M is $GK(I + GK)^{-1}$. The design goal was to keep any peaks of $\mu_{\text{app}}[KG(I + KG)^{-1}]$ and $\mu_{\text{app}}[GK(I + GK)^{-1}]$ below values of 5 dB. In the final stages of the design, single-loop gain and phase margins were checked and direct checks of stability through eigenvalue analysis made at many flight conditions away from the design point.

Rate-Command Design

The linear design model with delays cascaded to the input and output channels formed the aircraft model used in the design method [G in Eq. (2)]. The inputs to the helicopter model are the commanded main-rotor collective and cyclic inputs ($\Delta\theta_0$, $\Delta\theta_{1s}$, $\Delta\theta_{1c}$) and the commanded tail rotor collective pitch $\Delta\theta_{0_{\text{TR}}}$. The main-rotor inputs define the pitch of the kth rotor blade through

$$\Delta\theta_k = \Delta\theta_0 + \Delta\theta_{1s}\sin(\psi_k) + \Delta\theta_{1c}\cos(\psi_k) \tag{8}$$

where ψ_k is the azimuth of the rotor. The delay at these inputs is 50 ms, which was approximated by first-order Padé models. The expected source of this delay was due to 10 ms of compu-

tational delay, 10 ms of zero-order-hold delay, and 30 ms of actuator delay. The computational delay and zero-order-hold delay were based on a 50-Hz sample rate. The measurements are the roll rate p, pitch rate q, yaw rate r, and vertical velocity w. First-order Padé models approximated the output delays, which were 50 ms for the p, q, and r measurements, and 20 ms for the w measurement. The delay in the attitude-rate measurements assumes a third-order Bessel filter to attenuate the 4/rev noise from the rotor by 90%. The roll, pitch, yaw, and heave axes were all designed to be rate-command response types.

A characteristic of the design method is that some of the closed-loop poles always end up as the stable complement of the open-loop poles.[6] That is, for any stable open-loop pole, there will be a stable closed-loop pole at the same position in the s plane, whereas for any unstable open-loop pole, there will be a stable closed-loop pole that is a reflection of the unstable open-loop pole about the imaginary axis. This limitation does not cause problems if pole placement is not a requirement or, if by luck, the open-loop poles happen to be in acceptable positions. Unfortunately, neither of these conditions existed for this design problem. The ADS-33C requires that the low-frequency lateral and longitudinal poles be located in certain regions of the s plane. Reconsidering Table 1, we see that the open lateral poles at $-0.13 \pm j0.52$ would produce closed-loop poles at this same position, which would be too lightly damped to meet the ADS-33C level-1 requirements of 35% damping. To overcome this problem, small feedback gains from the roll and pitch rates to the cyclic pitch inputs were used to modify the low-frequency eigenvalues of the design model by repositioning these poles. This modified design model was then used in the design technique to produce the controller, which, when applied to the *unmodified* design model, yielded closed-loop eigenvalues near the desired positions. The working assumption is that very small gains are required to adjust the design model and the feedback of the controller is high enough to overcome the error between the modified and unmodified design models.

To place the design model poles, the eigenstructure assignment technique in Ref. 13 was used, along with an eight-state, quasistatic-rotor model. The eight-state model was used since the eigenvalues being moved are the low-frequency body modes. The roll and pitch rate act as outputs and the cyclic swashplate motions as inputs. Since there are two inputs and two outputs, two eigenvalues can be arbitrarily placed, as well as two elements of two eigenvectors. The undesirable eigenvalues at $-0.13 \pm j0.52$ were assigned new positions at $-0.20 \pm j0.48$ (40% damping), whereas the eigenvector elements associated with the yaw rate and vertical rate were given values identical to their open-loop values. This choice kept the yaw and vertical modes virtually unchanged and allowed the longitudinal and lateral modes to vary, all with relatively small gains. The final feedback law from the eigenstructure assignment is $\Delta\theta_{1s} = 0.051p + 0.077q$ and $\Delta\theta_{1c} = -0.017p + 0.005q$, where the swashplate inputs are in degrees and the body rates in deg/s. The repositioning of the lateral mode did not move the longitudinal mode into an undesirable position, and thus the pole requirements in the ADS-33C were met.

These gains were used to form a modified design model to which the design technique was applied. The sensitivity weight function for the design is

$$W_S(s) = \frac{100}{100s + 1}\,\mathrm{diag}[10.3,\ 9.0,\ 16,\ 5.7] \tag{9}$$

while $W_T(s)$ is a 4×4 identity. The control-input weight function is

$$W_W(s) = \mathrm{diag}\left[\frac{s + 0.01}{s + 10},\ \frac{s + 0.015}{s + 15},\ \frac{s + 0.02}{s + 20},\ \frac{s + 0.02}{s + 20}\right] \tag{10}$$

The characteristic $1/s$ behavior near the crossover of the elements of W_S is important for control-law disturbance rejection and good tracking below the crossover frequency. The W_S function dominates the performance index in Eq. (1) and, therefore, forces S_O to have a low value in the low-frequency range. Above the crossover frequency, the W_T and W_W weight functions dominate the performance index and, therefore, force both T_O and W to roll off. Raising the gain on each element of W_S [e.g., doubling the gain in the first element in Eq. (9) from 10.3 to 20.6] tends to increase the crossover of the feedback. Lowering the pole and zero pair proportionally in W_W [e.g., halving the pole and zero in the first element in Eq. (10) from 0.01 and 10 to 0.005 and 5.0] tends to lower the crossover of the feedback. Choosing W_T as the identity proved satisfactory; however, if even more roll off of T_O is required, then W_T should be chosen with a shape that increases at high frequency. The parameters of these weight functions were selected to give crossover frequencies near 4, 2.5, 4, and 2 rad/s for the roll, pitch, yaw, and vertical axes, respectively, which meet the disturbance rejection criteria in ADS-33C.

The full-order control law has 39 states: 23 states from the design model, 8 states from the time delay approximations, and 8 states from the weight functions. The full-order control law was reduced to 19 states using frequency-weighted balanced realizations. The weights in the model reduction were diagonal transfer-function matrices at both the input and the output, with each element defined as $10s + 1/0.2s^2 + 1.2s + 1$. This weighting placed more emphasis in the frequency range between 1 and 40 rad/s than outside of this region. Compensator reductions lower than 19 states produced significant differences in the on-axis magnitude and phase characteristics of the closed-loop roll channel below 40 rad/s.

The singular values of the sensitivity function are shown in Fig. 2. The reader is reminded that these plots and all other closed-loop information that follows were generated using the *unmodified* design model. The spread between singular values is due to having different bandwidths in each channel. The small sensitivity at low frequency indicates that good tracking of the body rates will occur for a commanded step input (i.e.,

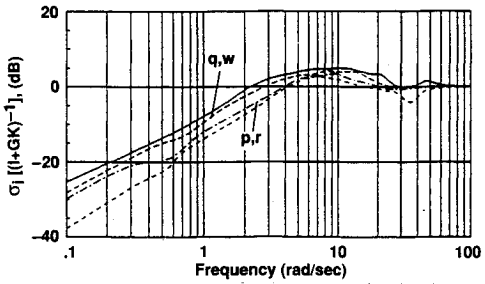

Fig. 2 Singular values of the sensitivity transfer-function matrix.

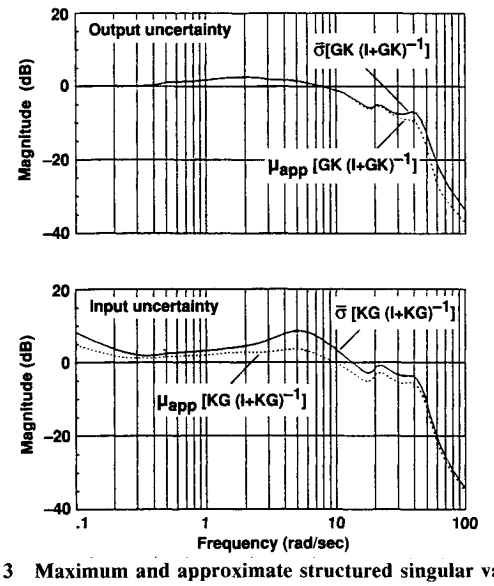

Fig. 3 Maximum and approximate structured singular values.

rate-command response). At low frequency, the two largest singular values are primarily associated with the pitch and vertical motions. That is, disturbances entering the q and w channels primarily reveal themselves at the output through these two channels. Thus, the pitch and heave axes have attenuation of disturbances below 2 rad/s. The two lowest singular values are associated with the roll and yaw rate and they have attenuation of disturbances below 4 rad/s.

The maximum singular values and approximate structured singular values for the output and input uncertainty models are shown in Fig. 3. The μ_{app} does not exceed 5 dB for both uncertainty models. The single-loop gain margins were calculated by opening channels, one at a time, at the plant input and output. The phase margins with the p, q, r, and w channels opened one at a time are 55, 50, 57, and 66 deg, respectively, whereas the gain margins for these channels are 9.0, 8.8, 8.0, and 14 dB, respectively. The phase margins with the $\Delta\theta_0$, $\Delta\theta_{1s}$, $\Delta\theta_{1c}$, and $\Delta\theta_{0_{TR}}$ channels opened are 71, 51, 52, and 46 deg, respectively, whereas the gain margins for these respective channels are 12, 10, 9.2, and 8.3 dB, respectively. The stability of the feedback was also checked using several linearized models away from the design condition. Four parameters were varied in combination to give 72 different flight conditions: rotor speed (24, 27, and 30 rad/s), flight speed (1 knot forward, 30 knots forward, 15 knots right, and 15 knots left), air density (0.00238 and 0.00204 slug/ft^3), and gross weight (14,000, 16,800, and 20,000 lb). No significant destabilization of any of the rotor modes appeared in any of the flight conditions.

The Section 3 hover criteria in ADS-33C most affected by the compensation design are the low-frequency pole placement requirement and the disturbance rejection requirements just discussed. The former was circumvented by an ad hoc method. The latter was achieved by increasing the crossover frequency, while simultaneously not destabilizing any of the rotor modes of the system. On-axis prefiltering was used to attempt to meet the remaining Section 3 hover requirements in ADS-33C, since they are response characteristics. Most of the level-1 Section 3 hover requirements in ADS-33C were met, with the notable exception of the yaw attitude quickness requirements, which was due to insufficient tail rotor power. The level of feedback gain also proved high enough to yield level-1 decoupling when the on-axis prefilters were included.[6,7]

Table 2 shows the prefiltering for each axis. These transfer functions were chosen to shape the response of the system with the compensation applied to the nonlinear model. The pitch-axis prefilter was needed to remove unnecessary overshoot in this axis, whereas the vertical-axis prefilter adjusts the heave time constant to 2 s. The yaw-axis prefilter counteracts distortions that arose when using the nonlinear model that were not present with the linearized model. The compensation was designed using the linear model, which does not have the rpm degree of freedom. However, the response was checked on the nonlinear model, which does have this degree of freedom.

Differences also arose in the roll axis when using the linearized model as opposed to the nonlinear model. The roll prefilter was used to make a small adjustment to the roll response. Figure 4 shows the small-amplitude roll requirement

Table 2 Control design prefiltering

	Rate
Roll	$\dfrac{(s/10)^2 + [2(0.7)/10]s + 1}{(s/8)^2 + [2(0.45)]/8s + 1}$
Pitch	$\dfrac{s/8 + 1}{s/4 + 1}$
Yaw	$\dfrac{(s/3.1)^2 + [2(0.7)/3.1]s + 1}{(s/2.6)^2 + [2(0.5)/2.6]s + 1}$
Vertical	$\dfrac{s/5 + 1}{s/0.5 + 1}$

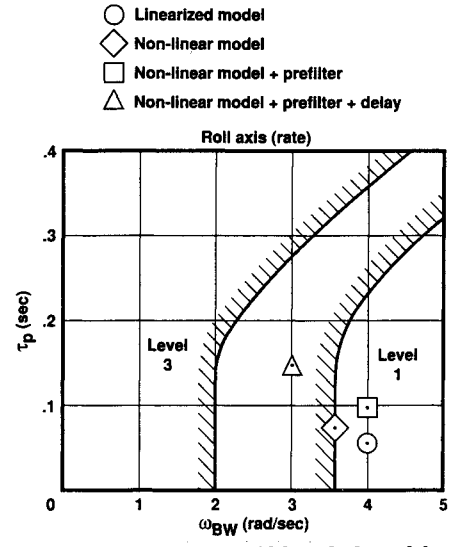

Fig. 4 Roll-axis bandwidth and phase delay.

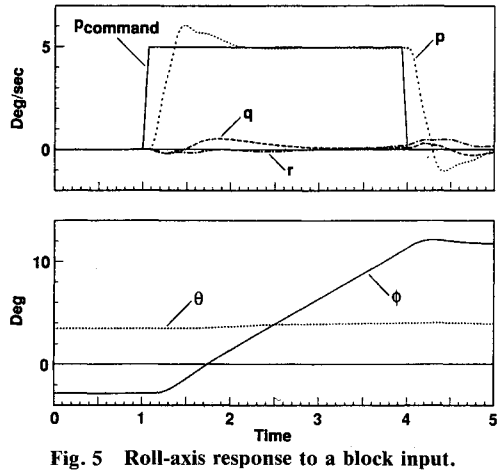

Fig. 5 Roll-axis response to a block input.

from ADS-33C. With the roll-attitude frequency plot, the bandwidth ω_{BW} is the lesser of the phase and gain bandwidth. The phase bandwidth $\omega_{BW_{phase}}$ is at the frequency of the -135 deg phase, whereas the gain bandwidth $\omega_{BW_{gain}}$ occurs at the frequency where the gain is 6 dB larger than the magnitude at the -180 deg phase.[1] The phase delay is

$$\tau_P = \frac{|180 \text{ deg} - \Phi_{2\omega_{180}}|}{57.3(2\omega_{180})} \tag{11}$$

where $\Phi_{2\omega_{180}}$ is the phase at twice the frequency of the -180 deg phase ω_{180}. The closed-loop system using the linear model without prefiltering has a 4.0 rad/s bandwidth, but this bandwidth drops to 3.5 rad/s when the nonlinear model is used. The closed-loop system using the nonlinear model with the prefilter restores the design to a 4.0 rad/s bandwidth. Figure 5 shows the nonlinear closed-loop roll response to a 5 deg/s roll-rate command block input. The system exhibits rate-command behavior and undergoes 15 deg of roll-attitude change with very little coupling to the pitch axis. The 20% overshoot in the roll rate is a consequence of meeting the attitude quickness requirements in the design specification.

Simulation Experiment

The control design was evaluated on the vertical motion simulator at NASA Ames Research Center. The evaluation pilot is located in a cab that pivots on a translating platform, which provides large-amplitude motion cues in 6 degrees of freedom. The cab is equipped with standard instruments and conventional helicopter controls, a center cyclic control, pedals, and side-arm collective control. For the design, the stick sensitivities were set to 15 deg/s/in. in roll and 10 deg/s/in. in

pitch. One inch of pedal motion gave 20 deg/s of commanded yaw motion, whereas 1 in. of collective gave 20 ft/s of vertical motion. The cab had three visual windows in the front, the right, and the lower right of the cab.

The visual system time delay is approximately 85 ms, whereas the simulator motion time delay is 70 ms in pitch and roll, 110 ms in yaw, and 160 ms in heave. The symbol labeled "Nonlinear + Prefilter + Delay" in Fig. 4 shows the approximate effect of this delay on the design, which is a loss of roll bandwidth. In addition to these time delays, the visual scene lacked microtexture, thus degrading the visual cue environment. These facts serve to remind the reader of the fidelity limitations of the simulation environment and that the purpose of the simulation was only to emphasize some features of the design for future design development and not strictly to validate the design against ADS-33C. Task development was also based on the limited nature of the simulation environment.

The simulation-scene data base layout consisted of an east-to-west road, which ended at the intersection of a north-south road. Pylons of 80 ft with 10-ft alternating dark and light blue horizontal stripes were arranged in the data base to enhance the visual cue environment. A nose boom was also included in the visual scene to improve the pilots' ability to sense yawing motion. To test each axis, four tasks were evaluated: an acceleration-deceleration, bob-up and bob-down, hovering turn, and sidestep. Table 3 summarizes the procedure for each task, as well as the conditions that must be met during the task. The tolerances have two levels, desired and adequate, that were used in assigning the handling qualities ratings (HQR).[14]

Two pilots were used in the evaluation, and each was allowed several practice runs (typically, between 5 to 10) before data and pilot comments were taken. In addition, the basic UH-60 simulation model was flown through the tasks in the same manner to give the evaluator a more familiar reference point from which to make his comments. The UH-60 simulation model has a limited-authority stability augmentation system and flight path stabilization.

Table 3 Summary of tasks

Procedure:	Conditions:	
1) Hover at h = 30 ft	1) Peak 12 deg nose down from trim	
2) Accelerate to 50 knots	2) Peak 15 deg nose up from trim	
3) Decelerate to hover		
Performance standards:	[Desired]	[Adequate]
1) Final longitude deviation, ft	[−10, 5]	[−20, 10]
2) Altitude deviation, ft	[−15, 15]	[−15, 30]
3) Heading deviation, deg	[−10, 10]	[−15, 15]
Bob-up		
Procedure:	Conditions:	
1) Hover at h = 20 ft	1) Time at 35 ft <6 s	
2) Ascend to 35 ft	2) Time to complete entire task <15 s	
3) Acquire target for 2 s		
4) Descent to 10 ft		
Performance standards:	[Desired]	[Adequate]
1) Position deviation, ft	[10]	[15]
2) Altitude overshoot, ft	[5]	[8]
3) Acquisition deviation, deg	[−2, +2]	[−5, +5]
Hovering turn		
Procedure:	Conditions:	
1) Hover at h = 20 ft	1) Time limit <15 s	
2) Turn 180 deg		
3) Hover in new direction		
Performance standards:	[Desired]	[Adequate]
1) Position deviation, ft	[10]	[20]
2) Altitude deviation, ft	[−5, +5]	[−10, +10]
3) Heading deviation, deg	[−5, +5]	[−10, +10]
Sidestep		
Procedure:		
1) Hover at h = 20 ft		
2) Translate laterally		
3) Decelerate to new hover position		
Conditions:		
1) At least 15 knots for at least 4 s		
2) 15-deg peak bank angle during acceleration and deceleration		
Performance standards:	[Desired]	[Adequate]
1) Longitude deviation, ft	[−10, +10]	[−20, +20]
2) Altitude deviation, ft	[−10, +10]	[−20, +20]
3) Heading deviation, deg	[−10, +10]	[−20, +20]

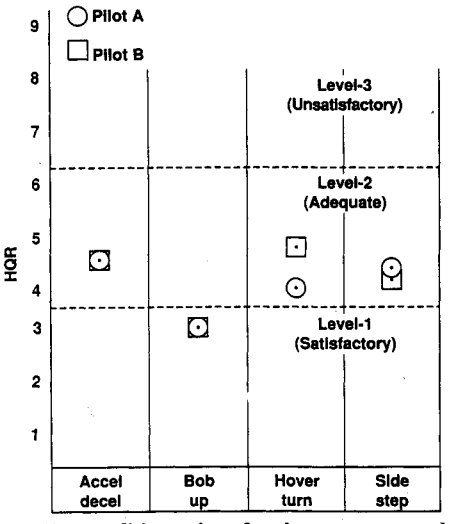

Fig. 6 Handling qualities ratings for the rate-command design.

Simulation Results

The handling qualities ratings for the tasks are summarized in Fig. 6. Concerning the simulator environment, the pilot comments were directed mostly at the difficulty of sensing longitudinal motion from the visual scene. The longitudinal motion was much more difficult to sense than lateral motion due to the lack of a complete view directly toward the right. Although the chin window allowed the ground to be visible, its small size and the lack of any refined texture on the ground made it only marginally effective in assessing motion. The pylons and nose boom were effective in enhancing the pilots' ability to sense lateral and yawing motion. The stripes on the pylons along with the horizon were useful cues for sensing vertical motion. However, the pylons were not always fully visible during each stage of each task, thus diminishing their effectiveness. An example of this effect occurred during the acceleration-deceleration, when the horizon was lost from the front window in the pitch-up condition.

Positive comments concerning the control system were directed toward the response characteristic in the pitch and yaw axes and the decoupling of the attitudes of the system. During the acceleration-deceleration, pilot A found that the "yaw axis and pitch axis were quite good," with no pitch-to-roll coupling noticeable and no yaw-axis attention required during the entire task. During the sidestep task, he found no adverse coupling in general and that the collective felt normal without feeding into the yaw axis. Yaw retention seemed good, and pitch control was easy, being used only for controlling fore-aft drifting. Pilot B found the longitudinal position requirement in the sidestep easy to meet because no inputs to pitch were required.

The characteristic of the control design that contributed most to the level-2 pilot ratings in Fig. 6 was an underlying pilot-induced oscillation (PIO) tendency in the roll axis. To avoid exciting this roll motion, pilot A altered his flying strategy to avoid sharp inputs, which he felt was unnatural. The PIO tendency became more apparent in the pitch-up attitude during acceleration-deceleration and during recovery from the sidestep maneuver. During the hovering turn and bob-up, he commented that a PIO tendency was underlying. The HQR = 4 for the hovering turn was primarily due to the poor visual cue environment for this task. Unlike pilot A, pilot B excited this roll motion more during the reversal of the hovering turn, which led to HQR = 5. Both pilots found height control difficult to manage in the high-attitude conditions at

the end of both the acceleration-deceleration and sidestep tasks. However, pilot B felt his effort to control height led him into the PIO tendency in roll. Figure 7 shows the body states of the configuration during the side step task for pilot B. Height oscillation is seen in the figure, followed by roll oscillations at 4–5 rad/s as the pilot attempted to stabilize his position at the end of the task. The oscillations depicted here are much more severe than those generated by pilot A.

The PIO tendency in roll was exacerbated by the normal velocity command response, which made controlling altitude difficult while in high-attitude conditions. However, it is expected that a redesign of the collective response to give a height velocity command response can be easily done using the design method just described. This redesign is not expected to remove the PIO tendency in roll, since it was sensed in the bob-up and hovering turn tasks, where pitch and roll attitudes stayed relatively small. Additionally, for the bob-up task, it was felt that if the pilot was forced to rush or turbulence was present, then the PIO tendency would manifest itself more forcefully.

Because of limited simulator time, isolating the exact cause of this PIO tendency was not possible. A contributing factor could be the motion and visual delays of the simulator that created a significant loss of roll bandwidth (Fig. 4). However, the level of aggressiveness of the tasks was not exceedingly high. Another possible source is the flap-regressing rotor mode, which is highly coupled to the roll motion and may lack adequate levels of damping. If we assumed enough simulation time, determining if the flap-regressing mode damping contributed to the roll PIO tendency would have been very difficult, due to an absence of a close connection between the parameters that define the compensation and damping. This lack of any simple direct connections to any feedback property is a major drawback of the design method, thereby making the resulting compensators impossible to adjust online.

Conclusion

A rate-command flight-control law was developed for a UH-60 configuration and evaluated by pilots on the vertical motion simulator at the NASA Ames Research Center. The design showed good response characteristics in the pitch and yaw axes and experienced good decoupling of the aircraft attitudes. Pilot ratings of less than satisfactory were due to an underlying pilot-induced oscillation tendency in the roll axis. The control law was synthesized using an H_2 loop-shaping method, and the resulting design met most of the Section 3 hover requirements in ADS-33C. The synthesis method eased the design of dynamic compensation through the mechanism of frequency-dependent weight functions, which allow the shaping of the sensitivity, complementary sensitivity, and control input matrices. The resulting compensation can be reduced to reasonable order and had good stability robustness properties with respect to rotor dynamics. The placement of low-frequency eigenvalues, as required in the design specification, could only be met through an ad hoc procedure. Also, as with most multivariable methods, the compensation is difficult to adjust online, due to an absence of a close connection between the parameters that define the compensation and the physical aspects of the design problem. During the simulation phase, the prefilters were the only means of adjusting the response of the design. Large differences will likely exist between actual helicopter characteristics and the design models used here and will require the adjustment of feedback compensation. To accommodate this expectation, a more fundamental understanding of feedback is necessary to allow online tuning.

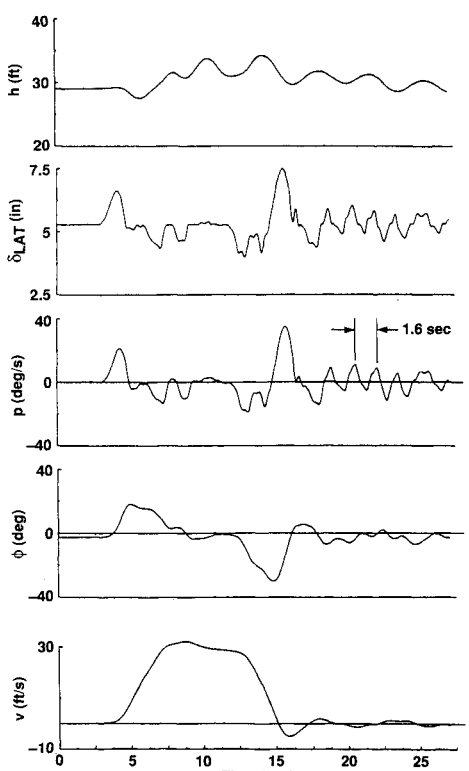

Fig. 7 Time history of the sidestep with pilot B.

Acknowledgments

The author wishes to thank M. M. Eshow for allowing this experiment to run in parallel with her experiment and for her assistance during the implementation of the design into the simulation model. The author is grateful to W. S. Hindson for his comments and suggestions during the setup of the simulation tasks and his evaluations. Finally, the author thanks R. Simmons for his time as an evaluation pilot.

References

[1]Anon., "Aeronautical Design Standard, Handling Qualities Requirements for Military Rotorcraft," U.S. Army Aviation Systems Command, St. Louis, MO, Aug. 1989.

[2]Miyajima, K., "Analytical Design of a High Performance Stability and Control Augmentation System for a Hingeless Rotor Helicopter," *Journal of the American Helicopter Society,* Vol. 24, July 1979, pp. 29–36.

[3]Garrard, W. L., Low, E., and Prouty, S., "Design of an Attitude and Rate Command Systems for Helicopters Using Eigenstructure Assignment," *Journal of Guidance, Control, and Dynamics,* Vol. 12, No. 6, 1989, pp. 783–791.

[4]Yue, A., and Postlethwaite, I., "H_∞ Design and the Improvement of Helicopter Handling Qualities," 13th European Rotorcraft Forum (Arles, France), Sept. 8–11, 1987.

[5]Tischler, M. B., "Digital Control of Highly Augmented Combat Rotorcraft," NASA TM-88346 or USAAVSCOM TR 87-A-5, May 1987.

[6]Takahashi, M. D., "Design of Flight-Control Laws for a UH-60 Helicopter in Hover Using an H_2 Loop-Shaping Method," NASA TM-103834, Oct. 1991.

[7]Takahashi, M. D., "Helicopter Flight-Control Design Using an H_2 Method," AIAA Paper 91-2753, Aug. 1991.

[8]Takahashi, M. D., "A Flight-Dynamic Helicopter Mathematical Model with a Single Flap-Lag-Torsion Main Rotor," NASA TM-102267, Feb. 1990.

[9]Ballin, M. G., and Dalang-Secretan, M.-A., "Validation of the Dynamic Response of a Blade-Element UH-60 Simulation Model in Hovering Flight," 46th Annual Forum of the American Helicopter Society, Washington, DC, 1990.

[10]Maciejowski, J.M., *Multivariable Feedback Design,* Addison-Wesley, Reading, MA, 1989.

[11]Chiang, R. Y., and Safonov, M. G., *Robust-Control Tool Box User's Manual,* Mathworks, Inc., South Natick, MA, 1988.

[12]Dailey, R. L., "Lecture Notes for the Workshop on H_∞ and μ Methods for Robust Control," 1990 American Control Conference (San Diego, CA), May 21–22, 1990.

[13]Andry, A. N., Shapiro, E. Y., and Chung, J. C., "Eigenstructure Assignment for Linear Systems," *IEEE Transactions on Aerospace and Electronic Systems,* Vol. AES-19, Sept. 1983.

[14]Cooper, G. E., and Harper, R. P., "The Use of Pilot Rating in the Evaluation of Aircraft Handling Qualities," NASA TN D-5153, April 1969.